A novel vortex flow reactor for the purification of B-phycoerythrin from *Porphyridium cruentum*

María J. Ibáñez-González[a,*], *Tania Mazzuca-Sobczuk*[a], *Rosa M. Redondo-Miranda*[a], *Emilio Molina-Grima*[a], *Charles L. Cooney*[b]

[a] *Department of Engineering, Agrifood Campus of International Excellence (CeiA3), University of Almeria, Almeria 04120, Spain*

[b] *Department of Chemical Engineering, Massachusetts Institute of Technology, 02139-4307 Cambridge, MA, USA*

ARTICLE INFO

Article history:
Received 10 January 2015
Received in revised form 10 March 2016
Accepted 30 March 2016
Available online 6 April 2016

Keywords:
Vortex flow reactor
Expanded bed
Péclet number
Protein
Adsorption
Purification

ABSTRACT

The purification of B-phycoerythrin from a concentrated extract of disrupted *Porphyridium cruentum* cells was carried out using a new vortex flow reactor design for protein purification. The reactor behaved as an expanded bed in the laminar vortices flow regime where the Streamline DEAE resin was expanded by the axial flow and stabilized by the vortex flow. After the broth culture was centrifuged and resuspended in the adsorption buffer, the concentrated extract of disrupted cells was directly loaded into the vortex flow reactor. The purification of B-phycoerythrin was carried out in two steps: adsorption in the expanded bed and elution from the settled bed. 142.0 mg of B-phycoerythrin was eluted representing a total recovery yield of 86.6%. Prior to B-phycoerythrin purification, the protein adsorption of the vortex flow reactor was characterized through hydrodynamic studies and a dynamic capacity measurement using a standard protein.

1. Introduction

Economic interest in the algae industry is ever increasing due to its relevance as a natural source of high added-value compounds such as pigments, specialty lipids, fatty acids, proteins, polysaccharides and phenolic compounds (Stengel et al., 2011). Among these products, natural pigments, present in phycobiliproteins, are of particular interest. Phycobiliproteins (phycocyanins and phycoerythrins) are used as fluorescent and pharmaceutical agents, as well as being used as natural protein dyes in the food and cosmetic industries (Sekar and Chandramohan, 2008). Phycocyanin is the food industry's most important blue-colored natural pigment, with applications in bubble gum production, milk products and jelly (Santiago-Santos et al., 2004). It has been suggested that red microalgae pigments could be used as food and cosmetic constituents (De Jesus Raposo et al., 2013), whereas the main potential for phycobiliproteins seems to be their use as natural dyes (Spolaore et al., 2006) although an increasing amount of research has additionally demonstrated their health-promoting properties and proposed a broad range of pharmaceutical applications (Richa et al., 2011). Phycoerythrin, which is red and fluorescent, can be used in fluorescence-based immunity assays and as non-radioactive markers in microscopy and DNA assays (De Jesus Raposo et al., 2013). Moreover, phycoerythrin extracted from *Porphyra haitanensis* has recently been described as having cancer-preventing potential due to its antioxidant properties (Pan et al., 2013). Among other organisms, the unicellular red algae *Porphyridium cruentum* is of special interest because it is a source of B-phycoerythrin (B-PE), which is commercially available as a fluorescent dye for flow cytometry and

* *Corresponding author at*: Department of Engineering, University of Almeria, Agrifood Campus of International Excellence (CeiA3), Carretera de Sacramento, Almeria 04120, Spain. Tel.: +34 950015960; fax: +34 950015491.
E-mail address: mjibanez@ual.es (M.J. Ibáñez-González).
http://dx.doi.org/10.1016/j.cherd.2016.03.032

Nomenclature

$A^{545}_{supernatant}$	absorbance at 545 of the supernatant
$A^{545}_{whole\ cell}$	absorbance at 545 of the whole cell
$A^{750}_{whole\ cell}$	absorbance at 750 of the whole cell
Bi	Biot number $Bi = \frac{k_f \cdot d_p}{D_p}$
C	protein concentration in the reactor outlet ($g\,L^{-1}$)
C_0	protein concentration in the reactor inlet ($g\,L^{-1}$)
d	annular gap width $r_o - r_i$ (m)
D_p	diffusion coefficient of protein in the bulk ($m^2\,s^{-1}$)
D_{ax}	axial dispersion coefficient ($m^2\,s^{-1}$)
d_p	average adsorbent bead diameter (μm)
$d_{p_{min}}$	minimum adsorbent bead diameter (μm)
g	gravitational acceleration ($m\,s^{-2}$)
H	expanded bed height (cm)
H_0	settled bed height (cm)
K	consistency coefficient ($Pa\,s^n$)
k_f	film mass transfer coefficient
L	axial length of the reactor (m)
n	flow index
Pe	Péclet number $Pe = \frac{u_0 \cdot H}{D_{ax} \cdot \varepsilon}$
ri	inner (moving) cylinder radius (m)
ro	outer (stationary) cylinder radius (m)
Re	axial Reynolds number $Re = \frac{u_0 \cdot d}{\varepsilon \cdot \upsilon}$
S	gap area (cm^2)
Ta	Taylor number $Ta = \frac{\omega \cdot d \cdot r_i}{\upsilon}$
Ta_c	critical Taylor number $Ta_c = 41.02 \cdot \left(\frac{d}{r_i}\right)^{0.5} + 25.75 \cdot \left(\frac{d}{r_i}\right)^{0.5} + 1.85 \cdot \left(\frac{d}{r_i}\right)^{1.5}$
u_{mf}	minimum fluidizing velocity ($m\,s^{-1}$)
u_0	superficial velocity ($m\,s^{-1}$)
u_t	terminal fluidization velocity ($m\,s^{-1}$)

Greek letters

γ	shear strain rate (s^{-1})
σ^2_θ	variance
υ	cinematic viscosity ($m^2\,s^{-1}$)
ω	angular velocity of the inner cylinder (s^{-1})
τ	shear stress (Pa)
ε	bed porosity
μ_l	liquid viscosity (Pa s)
ρ_l	liquid density ($kg\,m^{-3}$)
ρ_p	density of the solid ($kg\,m^{-3}$)
Γ	VFR aspect ratio $\frac{H}{d}$
η	radius ratio $\frac{r_i}{r_o}$

Abbreviations

BSA	bovine serum albumin
B-PE	B-phycoerythrin
DEAE	diethyl aminoethyl
EB	expanded bed
EB-VFR	vortex flow reactor in expanded bed
PE	phycoerythrin
RTD	residence time distribution
VFR	vortex flow reactor

immunofluorescent staining (e.g. Invitrogen, Columbia Biosciences, AnaSpec). It consists of two dissimilar α- and β-polypeptide chains of approximately 17–20 kDa with a 1:1 stoichiometry as well as a third type of polypeptide with an apparent molecular mass of 30–33 kDa, called the γ-subunit (Glazer and Hixson, 1977; Swanson and Glazer, 1990). The native conformation of B-PE is that of very stable disk-shaped $(\alpha\beta)_6$-γ aggregates that form part of the phycobilisomes (Wilbanks and Glazer, 1993). pH-dependent structural conformations of B-PE extracted from *P. cruentum* have already been determined by Camara-Artigas et al. (2012).

Expanded bed adsorption chromatography is an alternative bioseparation technique that greatly reduces the number of purification steps required by capturing target molecules directly from particle-containing feedstocks (Chase, 1994). This technology presents certain problems, the porous plate at the bottom of the column is sometimes blocked by the feedstock particles and there is not good contact between the adsorbent and the liquid when the feedstock is viscous, so channeling occurs in the expanded bed.

Another option is the vortex flow reactor (VFR), which consists of a rotating solid cylinder inside a stationary outer cylinder. Above a critical rotation rate, the circular Couette flow bifurcates to a series of counter-rotating toroidal vortices, called Taylor vortices, also described as a vortex flow, resembling "donuts" stacked around the inner cylinder (Taylor, 1923). Each vortex has a size approximately equal to the annular space between the cylinders. The expanded bed in the VFR is produced by the axial flow and/or rotation rate of the inner cylinder. The rotational speed of the inner cylinder has the advantage of being independently variable of the axial velocity thus avoiding channeling and producing a stable expanded bed.

The use of VFRs for protein adsorption started in the early nineteen-nineties (Moore, 1994). Moore worked with a protein pattern from bovine serum albumin and introduced different percentages of Streamline DEAE adsorbent into the VFR (up to 50%) but this led to significant blockages of the reactor outlet by the resin. Ten years later, the VFR was used to obtain recombinant human α1-antitrypsin from a clarified *Escherichia coli* culture, which had been expressed (Ma and Cooney, 2004). To prevent resin entrainment, they designed a reactor outlet that occupied the entire annular space, decreasing the flow to the axial outlet. Ma and Cooney (2004) filled only 5% of the reactor volume with adsorbent, resulting in low productivities. In both studies, the resin was suspended due to the rotational speed of the inner cylinder rather than by the axial velocity. Both designs also incorporated a nylon membrane at the reactor outlet, necessary to prevent adsorbent from escaping, which meant that they could not work with unclarified broth cultures or biological extracts.

Resin blockage at the reactor outlet was overcome by changing the operating conditions of the vortex flow reactor and by eliminating the nylon membrane at the reactor outlet (Ibáñez-González and Cooney, 2007). Bed expansion was due to the axial velocity not to the rotational speed. If there was only rotation, the adsorbent would settle in the reactor. Although the adsorbent percentage in the reactor increased when the protein adsorption pattern was measured in an expanded bed, poor adsorption and low productivity resulted.

In the present work, a novel vortex flow reactor was designed, constructed and tested for an initial study of the adsorption and purification of B-PE from untreated feedstock: a concentrated extract of disrupted *P. cruentum* cells. The high residence times provided by the novel vortex flow reactor allow good adsorption of the target protein, B-PE. Feedstock particles pass through the expanded bed because the VFR has a large inlet, while B-PE is adsorbed onto the stable expanded

bed produced by the rotation rate. Purifying B-PE from unclarified protein extract would be impossible using traditional expanded bed columns due to the common problem of mesh blockage.

2. Materials

2.1. *The expanded-bed vortex flow reactor (EB-VRF)*

The VFR (Fig. 1) is formed from two concentric cylinders separated by a uniform gap. The outer clear acrylic cylinder (1) remains stationary while the inner stainless steel cylinder (2) is rotated by means of a variable speed motor (3) connected to a controller (Electro-Craft E652-M). The inner cylinder is attached to the base of the outer cylinder via a bearing. Outlet ports (4) are placed every 2 cm along the external wall of the outer cylinder, starting at a height of 15 cm from the base of the reactor. The speed of rotation varied from 0 to 300 rpm. Located at the bottom of the outer cylinder, 2 mm above the base of the reactor, there is: a liquid feed inlet (5) to the adsorption process, an outlet port (6) for removing the adsorbent and an outlet port to the elution process (7), which contains a nylon membrane to prevent adsorbent from escaping. The liquid outlet was located 4 cm above the expanded bed. Two peristaltic pumps (Watson Marlow 323, Cornwall, UK) provide a constant axial flow rate. Table 1 shows the VFR dimensions.

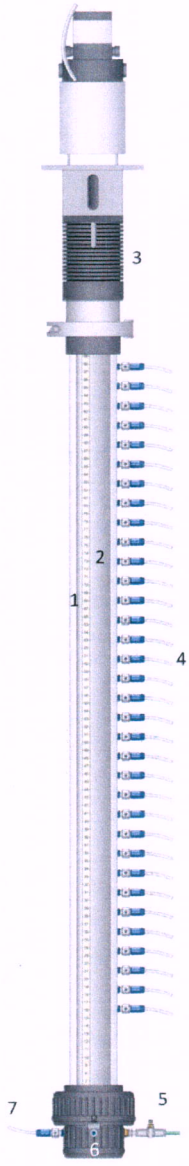

Fig. 1 – Schematic representation of the vortex flow reactor: (1) outer clear acrylic cylinder, (2) inner stainless steel cylinder, (3) variable speed motor, (4) outlet ports, (5) liquid feed inlet to the adsorption process, (6) outlet port for removing the adsorbent and (7) an outlet port to the elution process.

Table 1 – Geometric VFR dimensions.

r_o (inner radius of outer cylinder), cm	2.60
r_i (outer radius of inner cylinder), cm	2.15
L (height of the outer cylinder) cm	95
H (expanded bed height)	37–75
d (annular gap width, $r_o - r_i$), cm	0.45
S (gap surface area), cm^2	7.385
Γ (aspect ratio, H/d)	82–167
η (radius ratio, r_i/r_o)	0.81

2.2. *The adsorbent and standard protein for VFR characterization*

Streamline DEAE adsorbent from Pharmacia Biotech AB (Uppsala, Sweden) comprises 6% cross-linked agarose with an inert crystalline quartz core. The average adsorbent density is 1.2 g mL^{-1} and particle sizes range between 100 and 300 mm.

Bovine serum albumin (BSA) fraction V (A-7906) was obtained from Sigma Chemical Co. (St. Louis, MO, USA).

2.3. *Buffers*

The following buffers were employed:

- Adsorption buffer for BSA: 50 mM Tris–HCl, pH 7.5.
- Elution buffer for BSA: 0.5 M sodium chloride, 50 mM Tris–HCl, pH 7.5.
- Adsorption buffer for B-PE: 50 mM acetate, pH 5.5
- First elution buffer for B-PE: 250 mM acetate, pH 5.5.
- Second elution buffer for B-PE: 1 M acetate, pH 5.5.

Tris–HCl and acetate were obtained from Sigma Chemical Co. (St. Louis, MO, USA).

2.4. *Cell cultures*

The microalga *P. cruentum* was obtained from the culture collection of the Instituto de Ciencias Marinas (Puerto Real, Spain). The culture medium was Mediterranean Sea water enriched with f/2. The microalga was grown in a 20-L stirred-sparged photobioreactor. The culture's temperature was controlled at 25 ± 5 °C. The pH was maintained at 7.8 ± 0.1 via automatic carbon dioxide injections. The vessel was aerated at 0.5 v v^{-1} min^{-1}. The average irradiance at the bioreactor surface was 100 μE cm^{-2} s^{-1}. Four overhead TLD 36W/54 fluorescent lamps (Phillips, Amsterdam, The Netherlands) were used as the light source. At a dilution rate of 0.01 h^{-1}, B-PE productivity was 0.008 g L^{-1} day^{-1}.

3. Methods

3.1. Bed-expansion characterization

As suggested in the literature (Ibáñez-González and Cooney, 2007) the characteristics of the EB-VFR with the Streamline DEAE adsorbent were determined at room temperature (25 ± 5 °C). Adsorbent was added to the VFR at different settled bed heights (H_0) between 10 and 30 cm. The bed was equilibrated with the buffer at two different superficial velocities, 200 and 300 cm h^{-1}.

The terminal fluidization velocity, u_t, for the smaller beads, can be estimated by Stokes' law.

$$u_t = \frac{(\rho_p - \rho_l) \cdot d_{p_{min}}^2 \cdot g}{18 \cdot \mu_l} \quad (1)$$

where ρ_p is the density of the solid phase (kg m^{-3}), ρ_l is the density of the liquid phase (kg m^{-3}), $d_{p_{min}}$ is the minimum adsorbent bead diameter (μm), g is the gravitational acceleration (m s^{-2}) and μ_l is the viscosity of the liquid (Pa s).

The minimum fluidizing velocity, u_{mf}, is calculated using the equation from Levenspiel (1984):

$$u_{mf} = \frac{(\rho_p - \rho_l) \cdot d_p^2 \cdot g}{1650 \cdot \mu_l} \quad (2)$$

where d_p is the mean adsorbent diameter (mm).

3.2. Residence time distribution

Residence time distribution (RTD) was analyzed with a step tracer input at the bottom inlet of the EB-VFR and then by measuring the output signal at the EB-VFR outlet. A dilute acetone solution (0.25%, v/v acetone) was used as the tracer. The output signal was detected by UV absorption at 280 (nm) using a flow cell spectrophotometer (Jasco V-630, Tokyo, Japan).

The mean residence time and variance can be obtained by moment analyses of the RTD data. Considering the expanded bed of the VFR as an open vessel, the Péclet number (*Pe*) can be calculated from the following formula (Levenspiel, 1972):

$$\sigma_\theta^2 = 2 \cdot \left(\frac{1}{Pe}\right) + 8 \cdot \left(\frac{1}{Pe}\right)^2 \quad (3)$$

The Péclet number relates liquid convective transport to axial dispersion, defined as:

$$Pe = \frac{u_0 \cdot H}{\varepsilon \cdot D_{ax}} \quad (4)$$

where u_0 denotes the superficial liquid velocity (m s^{-1}), H is the expanded-bed height (m), ε is the bed voidage and D_{ax} is the axial dispersion coefficient (m^2 s^{-1}).

RTD studies were carried out in duplicate at two different superficial liquid velocities: 200 and 300 cm h^{-1}, and three different settled bed adsorbent heights: 10, 20 and 30 cm. The rotation rate was maintained constant at 25 rpm. The standard deviations of the duplicate assays represented the error.

3.3. Batch adsorption equilibrium with BSA

BSA solution was prepared in a Tris–HCl buffer (50 mM, pH 7.5). The starting BSA concentration was within the 0.5–5.0 g L^{-1} range. 0.5 mL of sedimented Streamline DEAE resin was mixed with 25 mL of BSA solution overnight in an orbital agitator (Heidolph UNIMAX 1010, Schwabach, Germany) at room temperature (25 ± 5 °C). The supernatant was removed and the residual BSA concentration was analyzed.

3.4. Dynamic capacity measurement with BSA

The breakthrough capacity was measured for the BSA and Streamline DEAE system. The dynamic capacity is the total amount of BSA adsorbed in the VFR per unit of adsorbent volume when the BSA outlet concentration is 10% of the inlet concentration and is calculated according to Chang and Chase (1995).

The BSA concentration in the loading sample was fixed at 2 g L^{-1} in order to get a linear response from the UV detector. The loading sample was prepared in 50 mM Tris–HCl buffer at pH 7.5 so that the BSA was negatively charged. The superficial liquid velocity fluidizes the Streamline DEAE adsorbent and the rotation (25 rpm) stabilizes the expanded bed in the EB-VFR. The dynamic capacity was measured while varying different experimental conditions such as superficial velocity (200–300 cm h^{-1}) and settled-bed height (10–30 cm).

3.5. Recovery of B-PE from P. cruentum

The B-PE purification flowchart is shown in Fig. 2 and involves the following steps: centrifugation of the microalgae culture broth, mixing the paste with buffer, five freeze/thaw cycles, B-PE adsorption in the EB-VFR and B-PE elution in the settled-bed VFR.

3.6. P. cruentum protein extract

The biomass was harvested from 7000 mL of culture using a centrifuge (Sartorius Sigma 4-15, Goettingen, Germany) operating at 5000 × *g* for 15 min. The cells were resuspended in buffer (50 mM acetate at pH 5.5). The final volume was 700 mL, meaning the cell concentration had increased by a factor of ten with respect to the initial cell culture concentration. The concentrated cell extract was subjected to five repeated freeze/thaw cycles of temperature shocks at −30 °C and 4 °C to release the B-PE.

3.7. B-PE and solid concentration

After each freeze/thaw cycle, a 1-mL aliquot was taken and the residue eliminated by centrifugation (Eppendorf mini spin plus, Hamburg, Germany) at 12,000 rpm for 5 min. The supernatant concentration of B-PE was calculated from absorbance measurements at 565, 620 and 650 nm using the simultaneous equations of Bennett and Bogorad (1973) and the extinction coefficients from Bryant et al. (1979).

The solid concentration was determined from 10 mL of concentrated cell extract before cell disruption. The sample was frozen and then lyophilized, before the lyophilized extract was finally weighed. The solid concentration was calculated by dividing the mass of lyophilized extract by the initial sample volume. The assay was performed in triplicate.

3.8. Expanded-bed vortex flow adsorption process for B-PE recovery

From concentrated extracts of disrupted cells, B-PE adsorption was performed using expanded-bed adsorption

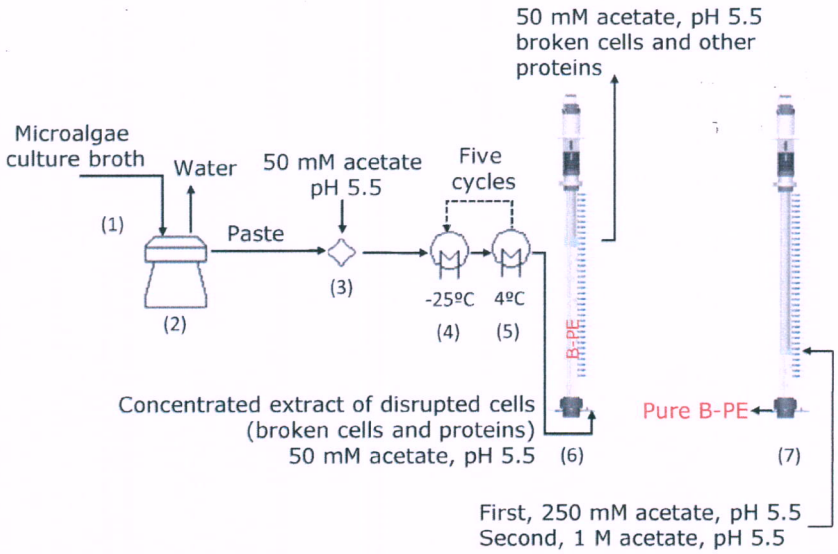

Fig. 2 – Flowchart for the purification of B-PE: (1) microalgae culture from photobioreactor, (2) centrifugation, (3) mixing, (4) freezing at −25 °C; (5) thawing at 4 °C, (6) B-PE adsorption in EB-VFR and (7) B-PE elution in settled-bed VFR.

chromatography on the VFR (shown in Fig. 1) operating at a influent flow rate of 22.4 mL min^{-1} (200 cm h^{-1}). The annular space of the VFR was filled with Streamline DEAE adsorbent to a height of 20 cm (135 mL) and equilibrated in upward flow with 50 mM acetate buffer at pH 5.5. The equilibration time lasted until the expanded bed appeared to be optically stable, this was at an expanded-bed height of 37 cm. Subsequently, the concentrated extract of disrupted cells (620 mL) was added at an identical linear flow rate. The expanded-bed height increased up to 64 cm in the EB-VFR (Fig. 3a). The effluent

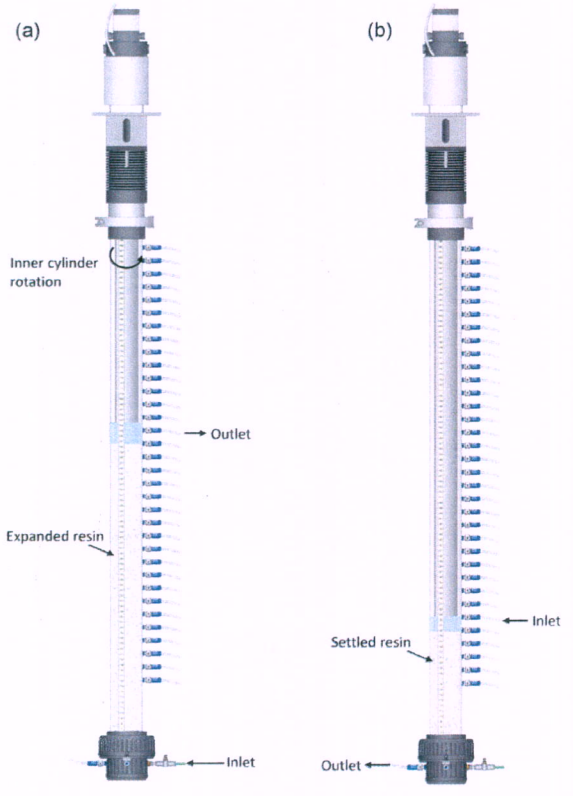

Fig. 3 – Visual description of the VFR for the adsorption and elution stages: (a) adsorption in the EB-VFR; (b) elution in the settled-bed VFR.

was collected in fractions using a Redifrac fraction collector (Pharmacia Biotech, Uppsala, Sweden). The rotation speed of the inner cylinder was 50 rpm.

During the feed application, only B-PE was adsorbed in the Streamline DEAE. Other proteins and broken cells were eluted. The adsorption process took 28 min. After the feed application, the annular space was washed with an equilibration buffer until no protein and no particles could be detected in the effluent for 150 min. The height of the expanded bed increased up to 79 cm.

Next, the variable speed motor was stopped and the bed allowed to settle before elution was performed in a packed-bed mode in the annular space of the VFR, operating at an axial velocity of 100 cm h^{-1} (Fig. 3b). The bound B-PE was eluted with 250 mM acetate buffer at pH 5.5.

Finally, the remaining adsorbed B-PE was completely eluted with 1 M acetate buffer at pH 5.5. The eluted fractions were then collected in the tube collector.

3.9. *Viscosity measurement of concentrated disrupted cell extract*

The concentrated extract viscosity of the disrupted cells was determined using a rotational viscometer (Brookfield DV-II + Pro Viscometer, LVF mode, spindle ULA-DIN-85, Middleboro, MA, US). The rheological parameters were obtained in duplicate with samples stored at room temperature. The fluid behavior (whether Newtonian or non-Newtonian) was classified through the analysis of the relationship between the shear strain rate and the shear stress (a rheogram), and the application of the Power Law Model, represented by the following equation:

$$\tau = K \cdot \gamma^n \tag{5}$$

where τ is the shear stress (Pa), K is the consistency coefficient (Pa s^n), γ is the shear strain rate (s^{-1}) and n is the flow index.

Through the Power Law model, the flow index (n) and consistency coefficient (K) are obtained by plotting $\log \tau$ (shear stress) versus $\log \gamma$ (shear strain rate) and determining the straight-line gradient. The flow index defines the behavior of

Table 2 – Bed porosity in the EB-VFR for various superficial velocities and settled-bed heights at 25 rpm.

Superficial velocity ($cm\,h^{-1}$)	H_0 (cm)		
u_0 ($cm\,h^{-1}$)	10	20	30
200	0.69	0.71	0.70
300	0.77	0.79	0.76

fluids as either Newtonian or non-Newtonian, where Newtonian fluids present an n value equal to 1, and non-Newtonian fluids have an n value different to 1. Rotation speeds of 20–80 rpm were used with increases of 10 and 20 rpm.

4. Results and discussion

4.1. *Expanded-bed characteristics*

The relation between the bed height of the Streamline DEAE adsorbent and the liquid flow rate in the VFR was assessed. Expanded-bed characteristics depend on the properties of the fluid, adsorbent and axial flow rate. In this work, the inner cylinder rotation rate does not have any influence on the height of the expanded bed because bed expansion is only produced by the axial flow rate and not by the rotation rate. The flow rate during adsorption must be between the minimum fluidization velocity, u_{mf}, and the terminal velocity (u_t) for the smaller beads in order to avoid adsorbent washout and maintain stable bed expansion. The u_{mf} value was calculated by Ibáñez-González and Cooney (2007) at 17 $cm\,h^{-1}$. The u_t for the minimum particle diameter was calculated in this work to be 392 $cm\,h^{-1}$. The bed-expansion variation for the Streamline DEAE at a rotation rate of 25 rpm was carried out for different settled-bed heights. Table 2 shows the bed's calculated void fraction and is almost independent of the settle bed height or aspect ratio. Similar results were obtained by Ibáñez-González and Cooney (2007) using an EB-VFR with a smaller aspect ratio.

4.2. *Residence time distribution*

The three major parameters influencing mixing in the liquid phase of the EB-VFR were identified as the aspect ratio (height of the stably expanded bed with respect to the annular width), the superficial velocity of the liquid stream and the rotation rate of the inner cylinder. The RTD studies were calculated experimentally to explore the hydrodynamic behavior of the EB-FVR using Streamline DEAE, operating at a constant rotation rate of 25 rpm while varying the axial velocity (200–300 $cm\,h^{-1}$) and aspect ratio (settled-bed height, between 10 and 30 cm). The Reynolds number and the Taylor number were estimated under these experimental conditions.

The Reynolds number was calculated for the range of superficial liquid velocities by means of Eq. (6). Its value varies from 3.6 to 4.9 between 200 and 300 $cm\,h^{-1}$, respectively. In the calculation, the viscosity of the water was used as an estimate of the dilute acetone solution's viscosity.

$$Re = \frac{u_0 \cdot d}{\nu \cdot \varepsilon} \tag{6}$$

where u_0 is the superficial axial velocity ($m\,s^{-1}$), d the annular gap width (m), ν the cinematic viscosity ($m^2\,s^{-1}$) and ε represents the fluid voidage in the reactor.

Table 3 – Péclet number of the RTD experiments and aspect ratio for various superficial velocities and settled-bed heights at 25 rpm ($Ta = 2.5 \cdot Ta_c$) in the EB-VFR.

H_0 (cm)	U_0 ($cm\,h^{-1}$)	H/d	Pe
10	200	43.0	17 ± 2
	300	58.0	26 ± 2
20	200	92.0	25 ± 1
	300	127.0	44 ± 4
30	200	133.3	21 ± 2
	300	166.7	27 ± 1

The Taylor number at a rotation rate of 25 rpm was calculated from Eq. (7) as having a value of 253.

$$Ta = \frac{\omega \cdot r \cdot d}{\nu} \tag{7}$$

where ω is the angular velocity (s^{-1}) and r_i the outer radius of the inner cylinder (m).

The critical Ta number to produce vortices can be calculated from Eq. (8) (Lee and Lueptow, 2001):

$$Ta_c = 41.02 \cdot \left(\frac{d}{r_i}\right)^{0.5} + 25.75 \cdot \left(\frac{d}{r_i}\right)^{0.5} + 1.85 \cdot \left(\frac{d}{r_i}\right)^{1.5} \tag{8}$$

The critical Taylor number for the configuration of the VFR used in this work was 102.

The experiments were carried out at a low rotation rate, 25 rpm ($Ta = 2.5 \cdot Ta_c$), in the laminar vortices flow regime, where $Ta < 15 \cdot Ta_c$ (Sczechowski et al., 1995). Under these operating conditions, Ibáñez-González and Cooney (2007) reported that the expanded bed is only due to the axial flow whereas the rotation rate has the function of stabilizing the particle suspension. If there is only an axial flow rate, between 200 and 300 $cm\,h^{-1}$, the expanded bed is not stable and channeling is observed in the annual space. The presence of laminar vortices stabilizes the expanded bed in the radial direction. As is indicated by the Reynolds number values (3.6–4.9) and Taylor number (253), the axial flow was dominant with respect to circular Couette flow and secondary vortex flow.

To normalize the effect of axial dispersion as a function of axial velocity, bed expansion and bed porosity, the Péclet number (Pe) was calculated (see Table 3). The Pe describes a possible influence of axial mixing on the performance of the EB-VFR. It is considered that the flow pattern is inclined to plug flow when $Pe > 20$. The expanded bed will behave similarly to a packed bed (Chang and Chase, 1995). The EB-VFR demonstrated plug flow behavior at 300 $cm\,h^{-1}$ and it could also be considered plug flow at 200 $cm\,h^{-1}$ due to the Pe number being higher than, or closer to, 20.

The Pe number increased with the superficial velocity for all settled-bed heights. Similar results were shown with different expanded bed systems (Thömmes et al., 1995; Li et al., 2004; Tong et al., 2003; Tong and Sun, 2001; Li and Chase, 2009).

The experimental Pe numbers were fitted to Moore's correlation (Moore and Cooney, 1995).

$$Pe^{-1} = 7.2 \times 10^{-3} \cdot \left(\frac{d}{r_t}\right)^{-0.28} \cdot Ta^{1.05} \cdot Ra^{-0.83} \cdot \left(\frac{2 \cdot d}{H}\right) \tag{9}$$

Moore's correlation was made without accounting for particles and considered the Pe number to increase with the height of the vortex flow reactor, when at a constant velocity. In this work, the variation in the experimental Pe number

with the settled-bed height presented a maximum at 20 cm while at constant velocity. Experimental data fitted well up to a settled-bed height of 20 cm (with an error below 25%). It could be considered from the model that particle presence in the EB-VFR has no influence on hydrodynamic behavior below a settled-bed height of 20 cm.

4.3. *Breakthrough capacity for BSA*

A standard protein, BSA, was used to determine the EB-VFR's operating conditions range for protein adsorption. A standard protein was more readily available and cheaper than the target protein of this work, B-PE.

Batch adsorption equilibrium experiments were conducted for BSA and Streamline DEAE at different initial BSA concentrations. The Langmuir isotherm was employed to fit the experimental data and to determine the maximum equilibrium adsorption capacity at 61 mg mL^{-1}. The EB-VFR's adsorption process efficiency was determined by measuring the dynamic capacity. This has to be close to the maximum equilibrium adsorption capacity to avoid loss of the target protein.

The dynamic capacity (mg of adsorbed BSA per mL of resin) was measured under the best hydrodynamic conditions for the EB-VFR, namely 200 and 300 cm h^{-1} at a settled-bed height of 20 cm, 60.4 mg mL^{-1} and 55.5 mg mL^{-1} were obtained, respectively. The dynamic capacity at 200 cm h^{-1} was closer to the maximum equilibrium adsorption capacity.

The mean residence times at 200 and 300 cm h^{-1} for a height of 20 cm were obtained from the moment analyses of the RTD data (Levenspiel, 1972), calculated to be 14.0 and 12.8, respectively. The dimensionless Biot number is defined as the relative effects of film mass transfer (k_f) and pore diffusion (D_p) on the protein adsorbent (Deen, 1998):

$$\mathrm{Bi} = \frac{k_f \cdot d_p}{D_p} \tag{10}$$

where d_p is the average adsorbent bead diameter (mm).

The Biot number was calculated following the indications of Ibáñez-González and Cooney (2007) for the BSA protein and the Streamline DEAE resin using a VFR with different aspect ratios at the same superficial velocity. They demonstrated that the dynamic capacity of the BSA on Streamline DEAE decreased with an increase in the superficial velocity due to pore diffusion limitations. In this work, the Biot number value was 12.1 and 13.6, for 200 and 300 cm h^{-1}, respectively. The results are in accordance with the literature data, because the protein, adsorbent and superficial axial velocity are similar; it is only changes in the VFR geometry which produce the small difference in the film mass transfer calculation (Ibáñez-González and Cooney, 2007). Therefore, the protein did not have enough time to penetrate into the pores when the residence time was decreased. Furthermore, this effect increases in parallel with an increase in protein size from BSA (66.3 Da) to B-PE (267 Da).

4.4. *B-PE extract*

Previously, various methods such as sonication and freeze–thawing for initial cell rupturing and extraction of the concentrated *P. cruentum* cell extract were considered. With sonication, it was possible to disrupt small volumes of cell samples but this did not work during the scaling up of the sample to 1 L. Freeze–thawing was the most suitable method for B-PE extraction (data not shown). As no standard method was available for maximum B-PE extraction from *P. cruentum*, the freezing and thawing temperatures were obtained from a phycocyanin protocol (Soni et al., 2006). Hence, the freeze–thawing pretreatment was carried out at −25 °C and 4 °C. The freeze–thawing extraction protocol performs well because it causes cells to swell and ultimately break due to the formation of sharp ice crystals during the freezing process which then contract during thawing.

Kilpatrick (1985) established a simple and qualitative procedure for determining the percentage of phycobiliprotein extracted, according to the equation:

$$\text{Extraction efficiency} = \frac{A^{545}_{\text{supernatant}}}{A^{545}_{\text{whole cell}} - A^{750}_{\text{whole cell}}} \cdot 100 \tag{11}$$

where A is absorbance, the superscripts 545 and 750 refer to the wavelengths (in nm); while subscripts supernatant and whole cell refer to the stage at which the absorbance was measured. The absorbance of the whole-cell extract (whole cells and large debris not separated from extracted proteins) was measured at 545 nm after each cycle. The correction factor at 750 nm was necessary because of incident light scattering from cell debris in the sample. Next, the sample was subjected to a cleanup step by centrifugation, and the absorbance of the resulting supernatant was measured at 545 nm.

The extraction efficiency was measured for each freeze/thaw cycle reaching 100% after five cycles, giving a B-PE concentration of 0.27 mg mL^{-1}. The ratio of A_{545}/A_{280} was 2.1, which means that there was a very low presence of other phycobiliproteins in the extract.

4.5. *Application of EB-VFR for B-PE recovery*

During the adsorption process, the concentration of B-PE and solids in the concentrated extract of disrupted cells was 0.27 mg mL^{-1} and 8.2 mg mL^{-1}, respectively. Optimal experimental conditions were selected: axial flow rate (200 cm h^{-1}), rotation rate (50 rpm) and the settled-bed height of the Streamline DEAE (20 cm).

The experimental conditions, axial flow rate and initial settled-bed height were selected from the results obtained for the BSA dynamic capacity experiments using Streamline DEAE. The highest dynamic capacity for BSA gave the best reactor operating conditions to purify B-PE. However, B-PE is physically much bigger than BSA and diffusion limitations could be significant.

The rotation rate of the inner cylinder was selected while taking into account the viscosity of the disrupted cell extract. Shear stress and shear strain rate were fitted to the Power Law model ($R^2 = 0.991$). The calculated values of the flow index (η) and the consistency coefficient (K) were 0.856 and 2.269 Pa s$^{0.856}$, respectively. The disrupted cell extract showed pseudoplastic fluid behavior, $\eta < 1$.

The adsorption process in the EB-VFR was carried out at 50 rpm. The shear strain rate of the EB-VFR was determined from the following equation:

$$\gamma\ (\mathrm{s}^{-1}) = \frac{\omega \cdot r_i}{d} \tag{12}$$

where ω is the angular velocity (s^{-1}), r_i the outer radius of the inner cylinder (m) and d the annular gap width (m).

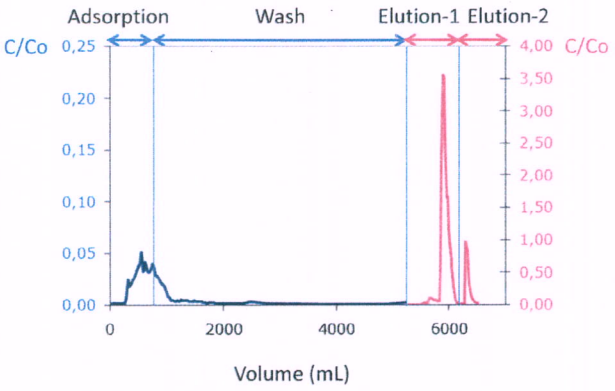

Fig. 4 – C/C_0 (B-PE concentration in the exit divided by the B-PE concentration in the concentrated disrupted cell extract) versus the volume for adsorption and washing stages using EB-VFR (blue line) and for the elution 1 (250 mM acetate, pH 5.5) and elution 2 (1 M acetate, pH 5.5) stages (pink line) using settled-bed VFR. (For interpretation of the references to color in this figure legend, the reader is referred to the web version of the article.)

The viscosity of the disrupted cell extract depends on the EB-VFR share strain rate and was calculated using the Power Law model (Eq. (5)) and assuming a crude extract density similar to that of water. Knowing the viscosity, 3.41 mPa s, the Taylor number was calculated to have a value of 156 using Eq. (7). The adsorption process was carried out in the laminar vortices flow regime, where $Ta = 1.5 \cdot Ta_c$.

From Eq. (7) it can be seen that the *Ta* number depends on the viscosity. The viscosity of the disrupted cell extract (3.41 mPa s) is greater than that of water (1 mPa s). Working at the same rotation rate, 25 rpm, an increase in the viscosity caused the *Ta* number to decrease below the critical Taylor number and the vortices regime disappeared. Therefore, an inner cylinder rotation rate higher than 25 rpm was selected for the disrupted cell extract in order to create vortices.

The *Pe* number was calculated under different experimental conditions for the Ta/Ta_c ratio = 2.5 (see Table 3). The *Pe* number at 200 cm h^{-1} for a settled-bed height of 20 cm was 25, indicative of plug flow behavior. Although the *Pe* number was not calculated for $Ta/Ta_c = 1.5$, its value should be higher than 25 because the *Pe* number increased when the Ta/Ta_c ratio was decreased due to the diminished turbulence of the fluid (Ma, 2003).

Fig. 4 represents C/C_0 versus volume during the B-PE purification process. C/C_0 is the ratio between the B-PE concentration at the outlet of the VFR (*C*) during the different stages (adsorption, wash and elution) and the initial B-PE concentration in the feed (C_0). The volume used in each stage is shown in Table 4. During the adsorption process, B-PE was linked into the resin until the B-PE concentration in the EB-VFR effluent reached 5% of the initial concentration ($C/C_0 = 0.05$). The dynamic capacity was calculated under these conditions. The dynamic capacity is the amount of B-PE linked per mL of resin, its value was 1.15 mg mL^{-1} ($C/C_0 = 0.05$). Literature data were obtained for clarified protein extract. Bermejo et al. (2003) purified B-PE from a traditional EB column where the adsorbent-B-PE load fraction was 0.88 mg B-PE mL^{-1} (the amount of initial B-PE per mL of resin). Although they did not report dynamic capacity data, its value should be equal to or lower than the load fraction, which is lower than the dynamic capacity obtained with the present EB-VFR. Ibañez-Gonzalez et al. (2013) patented a process whereby they purified B-PE using an EB pulsing column, achieving a dynamic capacity of 0.99 mg mL^{-1} ($C/C_0 = 0.07$). Although both dynamic capacities look similar, the dynamic capacity measured for the EB-VFR is higher than that of the EB pulsing column because its corresponding value was obtained at a lower C/C_0 ratio. Dynamic capacity in the EB-VFR is higher with respect to traditional and modified EB columns. Therefore, EB-VFR is capable of competing with EB columns and stands out as a technological improvement because it is possible to work directly with untreated protein extract.

The expanded-bed height in the EB-VFR was 64 cm; in this case, the number of continuous vortices was 64, which helped to obtain plug flow adsorption. After the application feed, the EB-VFR was washed with equilibration buffer until no protein and no particles could be detected in the effluent. At this point, the height of the expanded bed increased up to 74 cm due to the solids concentration of 8.2 mg mL^{-1}. Although the viscosity was reduced from 3.41 to 1 mPa s, it did not help to reduce the bed expansion in the VFR upon changing from the adsorption to wash stages.

The B-PE recovery, expressed as the percentage of the total amount of B-PE in the elute divided by the amount of B-PE loaded onto the resin, is shown in Table 4. The total recovery of B-PE from the purification process was calculated by adding all individual stage yields to be approximately 91.7%. The loss of B-PE during the adsorption and washing stages was only 5.1%. During the elution step in the settled-bed VFR, 120 mg of B-PE was obtained with 250 mM acetate buffer at pH 5.5. The calculated yield value was 73.2% with respect to the initial amount of B-PE. 22.0 mg of B-PE was recovered with 1 M acetate buffer at pH 5.5, which represented 13.4% of the initial B-PE. Together, both fractions gave a total B-PE recovery of 86.6%. Ibañez-Gonzalez et al. (2013) and Bermejo et al. (2003) both recovered higher yields in the first elution, 77.8% and 80.8% respectively, with clarified protein extract. However, for traditional columns, it would be impossible to purify B-PE

Table 4 – Volume, B-PE amount and B-PE yield in each VFR purification step: adsorption and wash in EB-VFR and the elutions (1 and 2) in the settled-bed VFR.

Purification stages	Volume (mL)	B-PE mg	B-PE yield (%)
Feed	620	164	100
Adsorption	620	3.0	1.8
Wash	4630	5.4	3.3
Elution 1	858	120.0	73.2
Elution 2	429	22.0	13.4
ΣElution 1 + Elution 2	1287	142.0	86.6
ΣAdsorption + Wash + Elution (1 and 2)	6537	150.4	91.7

Table 5 – Amount and yield of highly purified B-PE in the elution stages of the settled-bed VFR.

Elution stages	A_{545}/A_{280}	Purified B-PE (mg)	Purified B-PE yield (%)
Feed	2.1	164	–
Elution 1	>4	112.0	68.3
Elution 2	>4	16.0	9.8
ΣElution 1 + Elution 2	>4	128.0	78.1

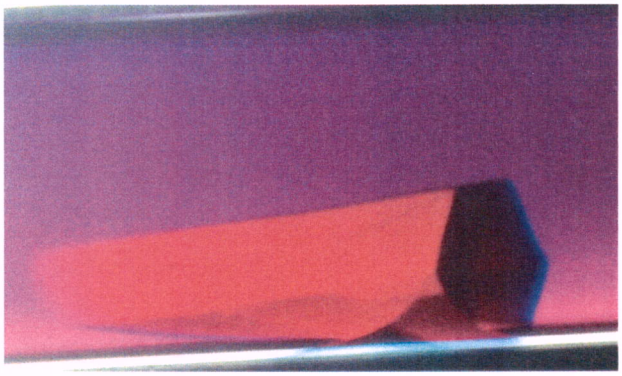

Fig. 5 – Photograph of a B-PE crystal grown via the capillary counter-diffusion technique from a purified fraction obtained in the VFR.

from unclarified protein extract due to the common problem of mesh blockage.

4.6. *Purity of the eluted fraction*

The purity of B-PE was determined from the (A_{545}/A_{280}) absorbance ratio. An A_{545}/A_{280} ratio >4.0 corresponds to highly purified B-PE. For the first and second elution buffer, 250 mM and 1 M acetate at pH 5.5, 112.0 and 16.0 mg of highly purified B-PE were obtained, respectively representing 68.3 and 9.8% of the initial B-PE (see Table 5). A total of 78.1% of highly purified B-PE was obtained.

A total of 128 mg of high purity B-PE were obtained with respect to the 142 mg of B-PE recovered in the elution stages. The purity ratio (A_{545}/A_{280}) of the concentrated extract of disrupted cells was 2.1 (see Table 5); this high value meant it was possible to obtain an elution of 90.1% of high purity B-PE.

B-phycoerythrin crystals from highly purified B-PE were obtained using the capillary counter-diffusion technique in accordance with the set-up described by Camara-Artigas et al. (2012). It is important to take into account that B-PE purity of the elution fraction was higher than 95% because it was possible to obtain high quality crystals, as shown in Fig. 5.

5. Conclusions

A novel VFR has been designed and characterized for protein adsorption experiments through hydrodynamic studies and dynamic capacity of a standard protein. The novel VFR was successfully applied to B-PE purification from *P. cruentum* disrupted cell extract and stands out as a technological improvement because it is possible to work directly with untreated protein extract. The novel vortex flow reactor is capable of competing with traditional and modified expanded-bed columns, but with the extra advantage of modifying and reducing the feed viscosity in pseudoplastic fluids, leading to a reduction in the external and internal mass transfer during the protein adsorption process.

Acknowledgements

This research was funded by the Spanish Ministry of Culture and Science and FEDER (EU), CTQ2006-05788 and BIO2008-06505. This work was performed by members of the BIO-173 Marine Microalgae Biotechnology Research Group of the Andalusian Regional Government (Spain). We would like to thank Ana Cámara-Artigas and her BIO-328 Protein Structures Research Group of the Andalusian Regional Government (Spain) for their support in obtaining the B-PE crystals.

References

Bennett, A., Bogorad, L., 1973. Complementary chromatic adaptation in a filamentous blue-green alga. J. Cell Biol. 58, 419–435.

Bermejo, R., Acién, F.G., Ibáñez, M.J., Fernández, J.M., Molina, E., Alvarez-Pez, J.M., 2003. Preparative purification of B-phycoerythrin from the microalga *Porphyridium cruentum* by expanded-bed adsorption chromatography. J. Chromatogr. B: Anal. Technol. Biomed. Life Sci. 790, 317–325.

Bryant, D.A., Guglielmi, G., de Marsac, N.T., Castets, A.-M., Cohen-Bazire, G., 1979. The structure of cyanobacterial phycobilisomes: a model. Arch. Microbiol. 123, 113–127.

Camara-Artigas, A., Bacarizo, J., Andujar-Sanchez, M., Ortiz-Salmeron, E., Mesa-Valle, C., Cuadri, C., Martin-Garcia, J.M., Martinez-Rodriguez, S., Mazzuca-Sobczuk, T., Ibañez, M.J., Allen, J.P., 2012. PH-dependent structural conformations of B-phycoerythrin from *Porphyridium cruentum*. FEBS J. 279, 3680–3691.

Chang, Y.K., Chase, H.A., 1995. Development of operating conditions for protein purification using expanded bed techniques: the effect of the degree of bed expansion on adsorption performance. J. Biotechnol. Bioeng. 49, 512–526.

Chase, H.A., 1994. Purification of proteins by adsorption chromatography in expanded beds. Trends Biotechnol. 12, 296–303.

De Jesus Raposo, M.F., De Morais, R.M.S.C., De Morais, A.M.M.B., 2013. Health applications of bioactive compounds from marine microalgae. Life Sci. 93, 479–486.

Deen, W.M., 1998. Analysis of Transport Phenomena. Oxford University Press, New York.

Glazer, A.N., Hixson, C.S., 1977. Subunit structure and chromophore composition of rhodophytan phycoerythrins. B-phycoerythrin and b-phycoerythrin. J. Biol. Chem. 252, 32–42.

Ibáñez-González, M.J., Cooney, C.L., 2007. Studies on protein adsorption in a vortex flow reactor. Process Biochem. 42, 1592–1601.

Ibañez-Gonzalez, M.J., Mazzuca-Sobczuk, T., Molina-Grima, E., 2013. Procedimiento de purificación de biomoléculas que utiliza cromatografía de adsorción en lecho expandido. ES Patent # 2383866.

Kilpatrick, K.A., 1985. The Development of a Method to Measure Marine Cyanobacterial Phycoerythrin Extracted in Solvents. Boston University.

Lee, S., Lueptow, R.M., 2001. Rotating reverse osmosis: a dynamic model for flux and rejection. J. Membr. Sci. 192, 129–143.

Levenspiel, O., 1972. Chemical Reaction Engineering. Wiley, New York.

Levenspiel, O., 1984. Engineering Flow and Heat Exchange. Plenum Press, New York.
Li, J., Chase, H.A., 2009. Characterization and evaluation of a macroporous adsorbent for possible use in the expanded bed adsorption of flavonoids from *Ginkgo biloba* L. J. Chromatogr. A 1216, 8730–8740.
Li, P., Xiu, G., Rodrigues, A.E., 2004. A 3-zone model for protein adsorption kinetics in expanded beds. Chem. Eng. Sci. 59, 3837–3847.
Ma, J., 2003. Characterization and Application of Vortex Flow Adsorption for Simplification of Biochemical Product Downstream Processing. Massachusetts Institute Technology.
Ma, J., Cooney, C.L., 2004. Application of vortex flow adsorption technology to intein-mediated recovery of recombinant human a1-antitrypsin. Biotechnol. Prog. 20, 269–276.
Moore, C.M.V., 1994. Characterization of a Taylor–Couette Vortex Flow Reactor. Massachusetts Institute Technology.
Moore, C.M.V., Cooney, C.L., 1995. Axial dispersion in Taylor–Couette flow. AIChE J. 41, 723–727.
Pan, Q., Chen, M., Li, J., Wu, Y., Zhen, C., Liang, B., 2013. Antitumor function and mechanism of phycoerythrin from *Porphyra haitanensis*. Biol. Res. 46, 87–95.
Richa, Kannaujiya, V.K., Kesheri, M., Singh, G., Sinha, R.P., 2011. Biotechnological potentials of phycobiliproteins. Int. J. Pharm. Biol. Sci. 2, 446–454.
Santiago-Santos, M.C., Ponce-Noyola, T., Olvera-Ramírez, R., Ortega-López, J., Cañizares-Villanueva, R.O., 2004. Extraction and purification of phycocyanin from *Calothrix* sp. Process Biochem. 39, 2047–2052.
Sczechowski, J.G., Koval, C.A., Noble, R.D., 1995. A Taylor vortex reactor for heterogeneous photocatalysis. Chem. Eng. Sci. 50, 3163–3173.
Sekar, S., Chandramohan, M., 2008. Phycobiliproteins as a commodity: trends in applied research, patents and commercialization. J. Appl. Phycol. 20, 113–136.
Soni, B., Kalavadia, B., Trivedi, U., Madamwar, D., 2006. Extraction, purification and characterization of phycocyanin from *Oscillatoria quadripunctulata* – isolated from the rocky shores of Bet-Dwarka, Gujarat, India. Process Biochem. 41, 2017–2023.
Spolaore, P., Joannis-Cassan, C., Duran, E., Isambert, A., 2006. Commercial applications of microalgae. J. Biosci. Bioeng. 101, 87–96.
Stengel, D.B., Connan, S., Popper, Z.A., 2011. Algal chemodiversity and bioactivity: sources of natural variability and implications for commercial application. Biotechnol. Adv. 29, 483–501.
Swanson, R.V., Glazer, A.N., 1990. Separation of phycobiliprotein subunits by reverse-phase high-pressure liquid chromatography. Anal. Biochem. 188, 295–299.
Taylor, G.I., 1923. Stability of a viscous liquid contained between two rotating cylinders. Philos. Trans. R. Soc. Lond. A 223, 289–342.
Thömmes, J., Weiher, M., Karau, A., Kula, M.-R., 1995. Hydrodynamics and performance in fluidized bed adsorption. Biotechnol. Bioeng. 48, 367–374.
Tong, X., Sun, Y., 2001. Nd-Fe-B alloy-densified agarose gel for expanded bed adsorption of proteins. J. Chromatogr. A 943, 63–75.
Tong, X., Xue, B., Sun, Y., 2003. Modeling of expanded-bed protein adsorption by taking into account the axial particle size distribution. Biochem. Eng. J. 16, 265–272.
Wilbanks, S.M., Glazer, A.N., 1993. Rod structure of a phycoerythrin II-containing phycobilisome. II. Complete sequence and bilin attachment site of a phycoerythrin γ subunit. J. Biol. Chem. 268, 1236–1241.